

Article

Characterizing Hydroxyapatite Deposited from Solution onto Novel Substrates in Terms of Growth Mechanism and Physical Chemical Properties [†]

Brid Murphy ^{1,2,*} , Jhonattan Baez ^{1,2} and Mick A. Morris ^{1,2}

¹ Advanced Materials & Bioengineering Research Centre (AMBER), Trinity College Dublin, Dublin 2, D02 CP49 Dublin, Ireland; baezj@tcd.ie (J.B.); morrism2@tcd.ie (M.A.M.)

² School of Chemistry, Trinity College Dublin, Dublin 2, D02 PN40 Dublin, Ireland

* Correspondence: murphb52@tcd.ie

[†] Presented at the 4th International Online Conference on Nanomaterials, 5–19 May 2023; Available online: <https://iocn2023.sciforum.net>.

Abstract: Bulk titanium and CoCr are the most common metals for use in orthopedic implants, but there are significant advantages in alternative substrates. Research in the last decade has focused on various alternatives; however, these materials are hindered by the adhesion of hydroxyapatite layers to non-bulk metal parts. Demonstrated in this work is the ability to grow hydroxyapatite on surfaces other than bulk metallic parts through the process and characterisation of coating properties. In this study, hydroxyapatite (HA) is grown from saturated solution onto thin titanium films and silicon substrates. Its efficacy is shown to be dependent on substrate roughness. The mechanism of the hydroxyapatite growth is investigated in terms of initial attachment and morphological development using SEM analysis. Characterisation of hydroxyapatite layers by XRD demonstrates how the hydroxyapatite forms from amorphous phases to preferential crystal growth along the [002] direction and TEM imagery confirms specific d-spacings. SEM-EDX and FTIR show adherence to known HA phases through elemental atomic weight percentages and bond assignment. All data are collated and reviewed through the lens of different substrates. The results suggest that once hydroxyapatite seeds, it grows identically regardless of substrate.

Keywords: hydroxyapatite; growth mechanism; characterisation



Citation: Murphy, B.; Baez, J.; Morris, M.A. Characterizing Hydroxyapatite Deposited from Solution onto Novel Substrates in Terms of Growth Mechanism and Physical Chemical Properties. *Mater. Proc.* **2023**, *14*, 34. <https://doi.org/10.3390/IOCN2023-14491>

Academic Editor: José Luis Arias Mediano

Published: 5 May 2023



Copyright: © 2023 by the authors. Licensee MDPI, Basel, Switzerland. This article is an open access article distributed under the terms and conditions of the Creative Commons Attribution (CC BY) license (<https://creativecommons.org/licenses/by/4.0/>).

1. Introduction

The most commonly used bulk materials for knee or hip replacements are chromium–cobalt or titanium alloys due to their mechanical strength and bio-inertness [1,2]. Although it is a common metal for use in orthopedic implants, there are concerns surrounding titanium’s use. The disadvantages of titanium parts include surface propagated cracks, titanium leeching, patient allergies, requirement to add other metals to the titania, and a problematic difference between the Young’s Modulus of titanium and natural bone [3–9].

Research over the last decade has focused on alternatives to titanium alloys. Polymers have considerable potential for use in orthopedic implants due to their mechanical properties and biocompatibility [10,11]. Experiments on epoxy-coated bamboo fibres found that it had potential as an implant material that would incur lower aseptic loosening post-joint replacement due to the fact that its stiffness was close to that of natural bone [12]. The development of materials for orthopedic parts is hindered by the need to add composites or nanomaterials to improve the adhesion of osteoinductive hydroxyapatite (HA) layers [13,14]. Reviews have called for solution-based HA deposition, which uses a material containing polymeric particles, to be deployed as a gateway to implementing polymeric based implants [15].

The research presented in this paper demonstrates the deposition of HA onto alternative substrates that would enable the effective creation of orthopedic implants from other materials. A novel method of solution deposition whereby phase, porosity and coating integrity are matched to existing HA properties is employed. Titanium coupons (Ti coupons) are used to model standard orthopedic parts. Novel substrates are crafted into the form of planar silicon and titanium thin films and are used to investigate the HA films formed on different surfaces. The data presented regarding titanium thin films show that HA can be deposited onto a <100 nm thick Ti film without the need to use bulk titanium, paving the way for the use of alternative substrates.

2. Materials and Methods

All materials and reagents were used as received. Monobasic potassium phosphate (KH_2PO_4) United States pharmacopeia (USP) reference standard, Honeywell Fluka hydrochloric (HCl) acid solution 6M, Tris(hydroxymethyl)-aminomethane (TRIS) ACS reagent, 99.8% sodium chloride (NaCl) BioXtra, and 99.5% calcium nitrate tetrahydrate ($\text{Ca}(\text{NO}_3)_2 \cdot 4\text{H}_2\text{O}$) ACS reagent were all obtained from Sigma Aldrich. KH_2PO_4 , TRIS and NaCl were mixed in deionized water (DIW) to yield a supersaturated phosphate solution. HCl was added to increase solubility stability and prevent precipitation. $\text{Ca}(\text{NO}_3)_2 \cdot 4\text{H}_2\text{O}$ was mixed with DIW to yield a supersaturated calcium solution. For deposition, the supersaturated solutions were combined before dilution by a factor of 5–10 and warming to 40–50 °C. The mixture was then agitated in a reaction vessel. Four-inch silicon wafers were used as received and a subset of these underwent e-beam evaporation–deposition (Temescal FC-2000) to generate 100 nm thin titanium films. Titanium coupons of Ti-6Al-4V alloy were also used. All substrates were submerged in hot basic solutions to increase their roughness and foster a more negatively charged surface to which calcium ions could attach [16,17]. Substrates were placed in the reaction vessel for deposition and then removed and rinsed with DIW. This process was repeated several times with fresh solutions to grow a coherent layer of HA at the solution–substrate interface.

Atomic force microscopy (AFM) was performed using an aXE-7, Park Systems AFM non-contact cantilevers. Scanning electron microscopy (SEM) data were collected using a Carl Zeiss Ultra Microscope equipped with an in-lens detector. An accelerating voltage of 5 to 10 kV was used. Energy-dispersive X-ray spectroscopy (EDX) spectra were acquired at 15 kV on an Oxford Inca EDX detector. X-ray diffraction (XRD) patterns were acquired using a Bruker Advance Powder Diffractometer (Cu- $\text{K}\alpha$ radiation with $\lambda = 1.5406 \text{ \AA}$, operating voltage of 40 kV and current of 40 mA). Measurements were performed in the 2θ range from 10° to 60° at steps of 0.004°. Transmission electron microscopy (TEM) was performed on an FEI Titan 80–300 microscope. Lamellae for TEM cross-section images were prepared on a Zeiss AURIGA Focused Ion Beam (FIB), obtaining accelerating voltages of 5–30 kV and ion beam currents of 50 pA–2 nA. Fourier transform infrared spectroscopy (FTIR) spectra were obtained using Perkin Elmer's Spotlight 200i benchtop device with attenuated total reflectance (ATR, 4000–500 cm^{-1} , 8 scans, and 4 cm^{-1} resolution diamond crystal).

3. Results

After the activation of the subjects, AFM was performed and XEI software was used to calculate roughness values in terms of average roughness (Ra) and peak-to-valley roughness (RPV) in nanometers for each substrate. The Ra of the novel substrates was <100 nm, with the RPV being 125–150 nm. Although this was lower than that of the titanium coupons, the roughness was in the same order of magnitude, as shown in Figure 1(1).

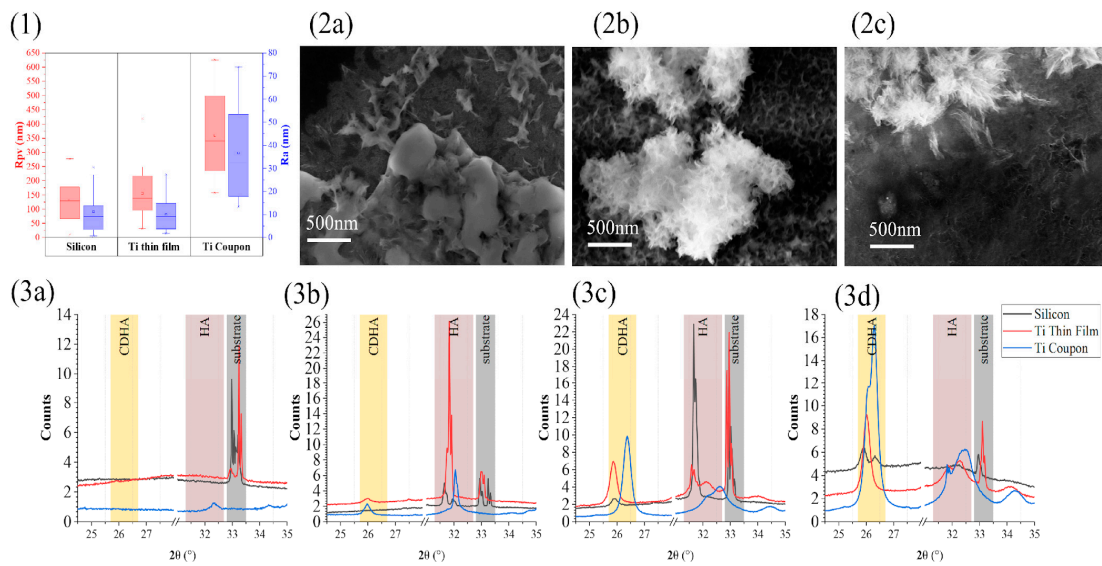


Figure 1. (1) The average roughness (Ra) and peak-to-valley (RPV) roughness of the three substrates post-activation as measured by atomic force microscopy; (2) Scanning Electron Microscopy images taken at 5 kv using inLens detector of samples after the first hydroxyapatite deposition run (a): silicon substrate, (b): titanium thin film substrate and (c): titanium coupon part. (3) X-ray diffraction patterns in terms of counts per second versus diffraction angle of 2θ collected for all three substrates silicon (grey line), Ti thin film (red line) and Ti coupon (blue line), (a): post-activation prior to any HA deposition, (b): post-2 HA deposition runs, (c): post-4 HA deposition runs and (d): post-6 HA deposition runs.

It was possible to see the effect of this roughness and surface activation after running HA deposition, whereby SEM topography had lighter areas of mineral deposits, as shown in Figure 1(2a–2c). All three substrates generated initial calcium attachment in discrete areas where there were surface groups for bonding. From this initial nucleation, heterogeneous growth of needle-like cobweb structure emerged as phosphate groups bonded to the calcium. Additionally, wider surface coverage was achieved identically for all three substrates, as shown in Figure 1(2a–2c). In order to delve deeper into the growth mechanism throughout HA deposition runs, XRD patterns were recorded after 2, 4 and 6 process runs, as shown in Figure 1(3). Both Ti thin films and silicon had substrate peaks around 33° . These diminished as the HA layer grew on the surface Figure 1(3a). These XRD diffractograms showed that the first detection of mineral growth was characteristic of HA planes (HA) such as [211], [112] and [310] around 32° . However, as the process continued, the mineral formed was calcium-deficient HA (CDHA), as indicated by the [002] plane at 26° [18–20]. After 2 process runs, the Ti thin film parts showed predominant sharp peaks of HA, but the silicon part did not show these until after 4 process runs, implying slower and less mineral growth for silicon, as shown in Figure 1(3b,3c). The Ti thin film samples followed the growth pattern of a typical titanium part through the emergence of CDHA and HA characteristic peaks at given stages in the deposition. The XRD study implied that (i) silicon had some CDHA phase, but that it also had the least counts and therefore the least material, and (ii) that the Ti thin film had a lower quantity of the same phases as the Ti coupon.

FIB lamellae were cut through HA films deposited onto all three substrate types and subsequent TEM cross-sectional analysis allowed for film thickness to be measured. Silicon HA coating measured roughly $1.5\ \mu\text{m}$, Ti thin films HA coating roughly $5\ \mu\text{m}$ and Ti coupon parts' HA coating roughly $6\text{--}7\ \mu\text{m}$ in thickness, as shown in Figure 2(4a–4c). TEM imagery showed HA with clear layers from the deposition cycles and pockets differing crystal orientations within an amorphous matrix, as shown in Figure 2(4d–4f). High resolution TEM images showed ordered lattice fringes for all three substrates and under analysis

these d-spacing were comparable to the XRD data peaks (CDHA of 0.34 nm and Pure HA 0.274–0.28 nm) Figure 2(4g–4i).

Further chemical analysis of the HA layers was carried out on samples post-full deposition. From FTIR it is evident that silicon substrate had the strongest indication of absorbed water in the HA layer, as shown in Figure 2(5a). All substrates had strong vibrational peaks within the known phosphate region of 700 to 1300 cm^{-1} , as shown in Figure 2(5b) [21,22]. All substrates demonstrated a matching ratio between the largest peak for $\nu^3 \text{PO}_4^{3-}$ and shoulder peak of $\nu^1 \text{PO}_4^{3-}$. Compared to the titanium samples, the silicon samples showed greater absorbance of HPO_4^{2-} in agreement with the XRD data. Only Ti coupons samples had a shoulder peak for pure HA. SEM analysis of the HA films post-deposition unveiled good coating integrity and similar morphologies for both Ti samples, but the silicon samples had less repeatable porosity and interconnectivity, as shown in Figure 2(8a–8c). The EDX analysis of these areas supported the calculation of the calcium-to-phosphate ratio (Ca:P) and oxygen atomic percentage (O at%) of these HA films, as shown in Figure 2(6a,6b). Silicon had the lowest Ca:P at 1.25 ± 0.12 , but the Ti thin film was 1.36 ± 0.14 , very close to a Ti coupon at 1.38 ± 0.07 , as shown in Figure 2(6b).

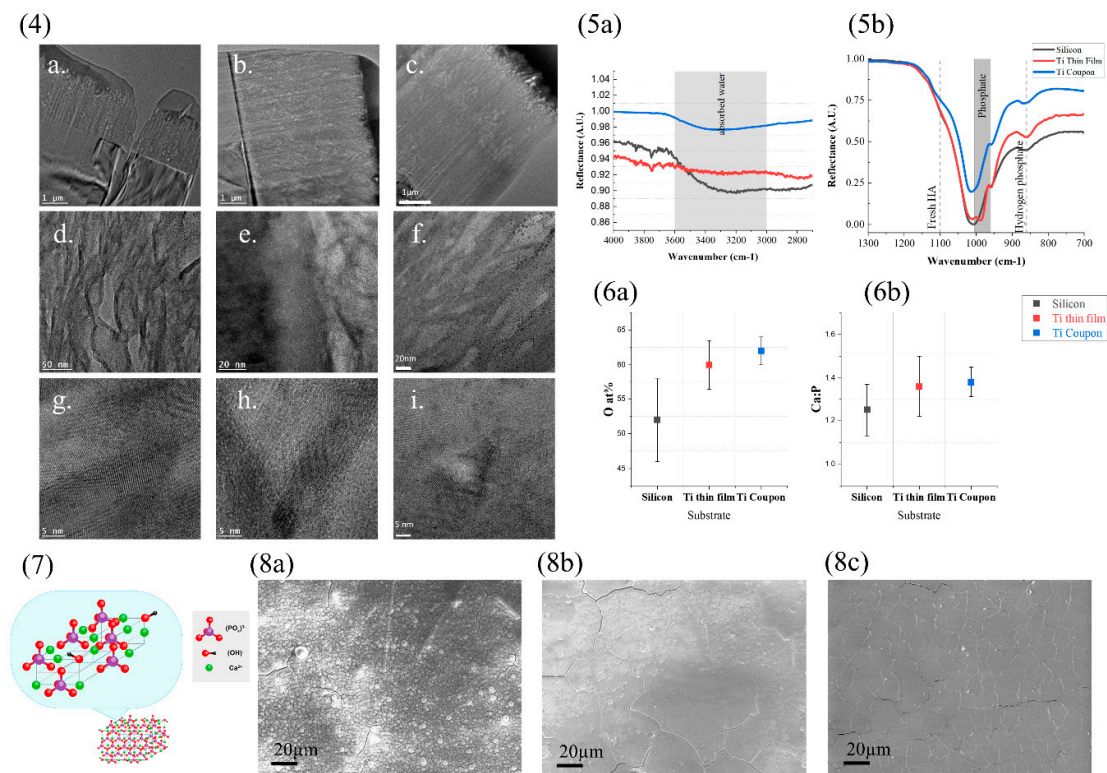


Figure 2. (4(a–i)): Transmission electron microscopy cross-sectional images of lamellae cut through HA layers, 1 μm scale, 50 nm scale bar and higher magnification nanometer scale; (a,d,g): cross-section of the HA layer over silicon substrate; (b,e,h): cross-section of the HA layer over Ti thin film substrate; (c,f,i): cross-section of the HA layer over Ti coupon part. (5): Fourier transform infrared spectra (a) in the absorbed water region of 4000–2000 cm^{-1} and (b) in the phosphate region of 1300–700 cm^{-1} of the full deposited HA layer over all three substrates: silicon (grey line), Ti thin film (red line) and Ti coupon (blue line). (6) Collated electron-dispersive X-ray data showing mean and error bars for the atomic percentage of (a) oxygen (O at%) and (b) calcium-to-phosphorus atomic percentage (Ca:P) found in the HA film deposited over silicon, Ti thin film and Ti coupon parts. (7) Crystal structure of hydroxyapatite. For better visualization, some atoms have been removed from the diagram. The diagram has been constructed from the literature [23,24] and using (8) scanning electron microscopy images taken at 5 kv using inLens detector of samples after 6 HA deposition runs; (a): silicon substrate; (b): Ti thin film substrate; and (c): titanium coupon part.

The unit cell of pure HA, formula $C_{10}(PO_4)_6(OH)$, had hydroxyl ions at the corners of the planes; additionally, phosphate anions and Ca^{2+} cations formed a hexagonal P63/m space group, as seen in Figure 2 (7). Other phases of HA exist, and from the data herein it became clear that HA films formed from this solution deposition process were a combination of phases. From literature, pure HA had a Ca:P of 1.67 and O at a % of 34.9%, amorphous calcium phosphate (ACP) $Ca_xHy(PO_4)_z \cdot nH_2O$ had a varying Ca:P and O at a %, and octacalcium phosphate (OCP) $Ca_8H_2(PO_4)_6 \cdot 5H_2O$ corresponded to a calcium-deficient HA phase which had a Ca:P of 1.33 with an O at a % of 39.7%. The Ca:P of all three samples heavily indicated the predominant formation of OCP, which supported the XRD observations. Samples in this study had O at a % of $52 \pm 6\%$ for silicon, $60 \pm 3.5\%$ for Ti thin film and $62 \pm 2\%$ for Ti coupon, meaning that all three possessed a higher oxygen content than the known phases. This implied the presence of ACP and hydrogen phosphates, but also the presence of adsorbed water and oxides around the lattice. Silicon samples showed the highest % of O, again implying the lowest pure HA content.

4. Conclusions

A successful method of deposition of hydroxyapatite films using a novel colloidal solution deposition process and its efficacy in creating non-bulk titanium parts was confirmed in this work. AFM analysis showed that although the two novel type substrates were less rough than a typical titanium part, SEM data proved that HA mineral deposits were generated after the first process run. XRD revealed the pathway by which HA grows within this process for a typical titanium part and that a Ti thin film parts follow this mechanism closely, but also that silicon has a slower growth mechanism. Through TEM analysis, the thickness and crystallinity of layers were compared. While silicon was found to have less material, all three substrates had crystalline pockets within an amorphous matrix. The chemical composition of the film, determined from FTIR and SEM-EDX data, showed that all three had ACP and OCP present with a limited proportion of pure HA, but that the silicon had higher impurities.

Overall, we confirmed that a Ti thin film can support the growth of an HA layer when matched to a Ti coupon part. This opens the possibilities of coating non-bulk metallic orthopedic implants.

Author Contributions: Conceptualization, B.M. and M.A.M.; methodology, B.M. and M.A.M.; investigation, B.M. and M.A.M.; writing—original draft preparation, B.M.; writing—review and editing, J.B. and M.A.M., visualization, J.B.; supervision, M.A.M. All authors have read and agreed to the published version of the manuscript.

Funding: This publication has emanated from research supported in part by a research grant from Science Foundation Ireland (SFI) and is co-funded under the European Regional Development Fund under Grant Number 12/RC/2278 and Grant Number 17/RC-PhD/3477. This research has been co-funded by DePuy Synthes (Ireland).

Institutional Review Board Statement: Not applicable.

Informed Consent Statement: Not applicable.

Data Availability Statement: Data is contained within the article.

Acknowledgments: We thank Lucie Hankey and Aidan Cloonan, for technical advice and scientific discussions. We thank the AML center and especially Raman Bekarevich for TEM analysis support.

Conflicts of Interest: The authors declare no conflict of interest.

References

1. Dobbs, H.S.; Scales, J.T. Behavior of Commercially Pure Titanium and Ti-318 (Ti-6Al-4V) in Orthopedic Implants. *Titan. Alloy. Surg. Implant.* **1983**, *B10*, 173–186. [[CrossRef](#)]
2. Keegan, G.M.; Learmonth, I.D.; Case, C. A Systematic Comparison of the Actual, Potential, and Theoretical Health Effects of Cobalt and Chromium Exposures from Industry and Surgical Implants. *Crit. Rev. Toxicol.* **2008**, *38*, 645–674. [[CrossRef](#)] [[PubMed](#)]

3. Grupp, T.M.; Weik, T.; Bloemer, W.; Knaebel, H.-P. Modular Titanium Alloy Neck Adapter Failures in Hip Replacement—Failure Mode Analysis and Influence of Implant Material. *BMC Musculoskelet. Disord.* **2010**, *11*, 3. [[CrossRef](#)]
4. Siddiqi, A.; Payne, A.G.T.; Silva, R.K.D.; Duncan, W.J. Titanium Allergy: Could It Affect Dental Implant Integration? *Clin. Oral Implants. Res.* **2011**, *22*, 673–680. [[CrossRef](#)] [[PubMed](#)]
5. Swiatkowska, I.; Martin, N.; Hart, A.J. Blood Titanium Level as a Biomarker of Orthopaedic Implant Wear. *J. Trace Elem. Med. Biol.* **2019**, *53*, 120–128. [[CrossRef](#)]
6. Niinomi, M.; Nakai, M. Titanium-Based Biomaterials for Preventing Stress Shielding between Implant Devices and Bone. *Int. J. Biomater.* **2011**, *2011*, 836587. [[CrossRef](#)]
7. Shi, Y.D.; Wang, L.N.; Liang, S.X.; Zhou, Q.; Zheng, B. A High Zr-Containing Ti-Based Alloy with Ultralow Young's Modulus and Ultrahigh Strength and Elastic Admissible Strain. *Mater. Sci. Eng. A* **2016**, *674*, 696–700. [[CrossRef](#)]
8. Tan, M.H.C.; Baghi, A.D.; Ghomashchi, R.; Xiao, W.; Oskouei, R.H. Effect of Niobium Content on the Microstructure and Young's Modulus of Ti-XNb-7Zr Alloys for Medical Implants. *J. Mech. Behav. Biomed. Mater.* **2019**, *99*, 78–85. [[CrossRef](#)]
9. Nakai, M.; Niinomi, M.; Zhao, X.; Zhao, X. Self-Adjustment of Young's Modulus in Biomedical Titanium Alloys during Orthopaedic Operation. *Mater. Lett.* **2011**, *65*, 688–690. [[CrossRef](#)]
10. Abitha, H.; Kavitha, V.; Gomathi, B.; Ramachandran, B. A Recent Investigation on Shape Memory Alloys and Polymers Based Materials on Bio Artificial Implants-Hip and Knee Joint. *Mater. Today Proc.* **2020**, *33*, 4458–4466. [[CrossRef](#)]
11. Saad, M.; Akhtar, S.; Srivastava, S. Composite Polymer in Orthopedic Implants: A Review. *Mater. Today Proc.* **2018**, *5*, 20224–20231. [[CrossRef](#)]
12. Ismail, N.F.; Shuib, S.; Romli, A.Z.; Saeid, N.H. Epoxy-Coated of Bamboo Fibre Reinforced Polymer Composite for Uncemented Total Hip Replacement (THR) Application. *J. Mech. Eng.* **2020**, *9*, 167–177.
13. Auclair-Daigle, C.; Bureau, M.N.; Legoux, J.-G.; Yahia, L. Bioactive Hydroxyapatite Coatings on Polymer Composites for Orthopedic Implants. *J. Biomed. Mater. Res. Part A* **2005**, *73A*, 398–408. [[CrossRef](#)] [[PubMed](#)]
14. Balasundaram, G.; Webster, T.J. An Overview of Nano-Polymers for Orthopedic Applications. *Macromol. Biosci.* **2007**, *7*, 635–642. [[CrossRef](#)]
15. Andrusova, N.N.; Zhavoronok, E.S.; Legon'kova, O.A.; Goncharova, A.S.; Kedik, S.A. Polymer–Mineral Compounds for Cementless Hip Replacement. *Polym. Sci. Ser. D* **2020**, *13*, 68–72. [[CrossRef](#)]
16. de Andrade, M.C.; Filgueiras, M.R.; Ogasawara, T. Nucleation and Growth of Hydroxyapatite on Titanium Pretreated in NaOH Solution: Experiments and Thermodynamic Explanation. *J. Biomed. Mater. Res.* **1999**, *46*, 441–446. [[CrossRef](#)]
17. Kim, C.; Kendall, M.R.; Miller, M.A.; Long, C.L.; Larson, P.R.; Humphrey, M.B.; Madden, A.S.; Tas, A.C. Comparison of Titanium Soaked in 5 M NaOH or 5 M KOH Solutions. *Mater. Sci. Eng. C Mater. Biol. Appl.* **2013**, *33*, 327–339. [[CrossRef](#)]
18. Keller, L.; Rey-Fessler, P. Nondestructive Characterization of Hydroxylapatite Coated Dental Implants by XRD Method. In *Characterization and Performance of Calcium Phosphate Coatings for Implants*; Horowitz, E., Parr, J.E., Eds.; ASTM International: Miami, FL, USA, 1992.
19. Ślósarczyk, A.; Paszkiewicz, Z.; Paluszkiwicz, C. FTIR and XRD Evaluation of Carbonated Hydroxyapatite Powders Synthesized by Wet Methods. *J. Mol. Struct.* **2005**, *744–747*, 657–661. [[CrossRef](#)]
20. Chappard, C.; André, G.; Daudon, M.; Bazin, D. Analysis of Hydroxyapatite Crystallites in Subchondral Bone by Fourier Transform Infrared Spectroscopy and Powder Neutron Diffraction Methods. *Comptes Rendus Chim.* **2016**, *19*, 1625–1630. [[CrossRef](#)]
21. Rehman, I.; Bonfield, W. Characterization of Hydroxyapatite and Carbonated Apatite by Photo Acoustic FTIR Spectroscopy. *J. Mater. Sci. Mater. Med.* **1997**, *8*, 1–4. [[CrossRef](#)]
22. Ślósarczyk, A.; Paluszkiwicz, C.; Gawlicki, M.; Paszkiewicz, Z. The FTIR Spectroscopy and QXRD Studies of Calcium Phosphate Based Materials Produced from the Powder Precursors with Different Ratios. *Ceram. Int.* **1997**, *23*, 297–304. [[CrossRef](#)]
23. Rujitanapanich, S.; Kumpapan, P.; Wanjanoi, P. Synthesis of Hydroxyapatite from Oyster Shell via Precipitation. *Energy Procedia* **2014**, *56*, 112–117. [[CrossRef](#)]
24. Pramatarova, L.; Pecheva, E. *Modified Inorganic Surfaces as a Model for Hydroxyapatite Growth*; Trans Tech Publications Limited: Stafa-Zurich, Switzerland, 2006.

Disclaimer/Publisher's Note: The statements, opinions and data contained in all publications are solely those of the individual author(s) and contributor(s) and not of MDPI and/or the editor(s). MDPI and/or the editor(s) disclaim responsibility for any injury to people or property resulting from any ideas, methods, instructions or products referred to in the content.